Reconstruction of the 2018 tsunamigenic flank collapse and eruptive activity at Anak Krakatau based on eyewitness reports, seismo-acoustic and satellite observations

A. Perttu, C. Caudron, J.D. Assink, D. Metz, D. Tailpied, B. Perttu, C. Hibert, D. Nurfiani, C. Pilger, M. Muzli, et al.

Earth and Planetary Science Letters 541 (2020) 116268

Contents lists available at ScienceDirect

Earth and Planetary Science Letters

www.elsevier.com/locate/epsl

Reconstruction of the 2018 tsunamigenic flank collapse and eruptive activity at Anak Krakatau based on eyewitness reports, seismo-acoustic and satellite observations

Perttu A.[a,*], Caudron C.[b], Assink J.D.[c], Metz D.[d], Tailpied D.[a], Perttu B.[e], Hibert C.[f], Nurfiani D.[a], Pilger C.[g], Muzli M.[h,a], Fee D.[i], Andersen O.L.[j], Taisne B.[a,e]

[a] Earth Observatory of Singapore, Nanyang Technological University, 50 Nanyang Avenue, Block N2-01a-15, 639798, Singapore
[b] Univ. Grenoble Alpes, Univ. Savoie Mont Blanc, CNRS, IRD, IFSTTAR, ISTerre, 38000 Grenoble, France
[c] Royal Netherlands Meteorological Institute (KNMI), R&D Seismology and Acoustics, PO Box 201, 3730 AE, De Bilt, the Netherlands
[d] Japan Agency for Marine-Earth Science and Technology, 2-15, Natsushima-cho, Yokosuka-city, Kanagawa, 237-0061, Japan
[e] Asian School of the Environment, Nanyang Technological University, 50 Nanyang Avenue, Block N2-01C-63, 639798, Singapore
[f] School and Observatory of Earth Sciences, University of Strasbourg and CNRS, 5 René Descartes Street, F-67084 Strasbourg cedex, France
[g] Federal Institute for Geosciences and Natural Resources (BGR), Stilleweg 2, 30655 Hanover, Germany
[h] Agency for Meteorology, Climatology and Geophysics (BMKG), Jl. Angkasa I No. 2 Kemayoran, Jakarta Pusat, DKI Jakarta 10720, P.O. Box 3540 Jkt., Indonesia
[i] Alaska Volcano Observatory, Geophysical Institute, University of Alaska Fairbanks, 2156 Koyukuk Drive, PO Box 757320, University of Alaska Fairbanks, Fairbanks, AK, 99775 USA
[j] Øystein Lund Andersen Photography, Bodø, Norway [1]

ARTICLE INFO

Article history:
Received 22 May 2019
Received in revised form 3 April 2020
Accepted 4 April 2020
Available online 23 April 2020
Editor: T.A. Mather

Keywords:
Anak Krakatau
remote monitoring
volcanic tsunami
infrasound
seismic
eyewitness

ABSTRACT

After several months of eruptive activity, the subaerial cone of Anak Krakatau collapsed on December 22, 2018. The landslide event generated a tsunami that had deadly consequences within the Sunda Strait in Indonesia. Such significant collapse events are common in the geologic record but are a rare phenomenon, in the instrumented record. However, these events can have a potentially large impact on society. We have reconstructed the collapse, along with the activity preceding and following it, by combining information from official reports, remote geophysical observations, and local eyewitness accounts. It appears that the collapse of Anak Krakatau's subaerial cone led to a drastic change in the eruptive style from continuous Strombolian explosions to sustained Surtseyan. Those changes are detectable in the seismo-acoustic measurements, which, when combined with eyewitnesses, allows us to reconstruct the timing and phenomenology of the sequence. Our analysis reveals that intense eruptive activity generated sustained infrasound, unusual but not unique at Anak Krakatau, starting approximately eight hours before the collapse. Within this timeframe, two seismic signals consistent with minor mass movements as well as a momentary quiescence were identified prior to the main collapse. The data presented here indicate that Anak Krakatau failed in one collapse event, producing a tsunami with multiple waves around the volcano, the last one being the largest. Following the collapse, three volcanic plumes could be clearly identified in the satellite data and by eyewitnesses, as well as spectral lines in the seismic data. These lines, observed up to 371 km, suggest a repeating energetic explosive source lasting for seven days. The collapse produced multiple infrasound arrivals observed at regional infrasound stations, but was not recorded on the regional hydroacoustic network. Our analysis of the eruptive sequence demonstrates that a detailed eruption chronology can be reconstructed using remote methods, even in the event of failure or destruction of local monitoring infrastructure. This event also highlights that tsunamigenic flank collapses can occur with little to no warning, and be difficult to interpret in real-time, as a significant amount of non-operational analysis was required after the event, to complete the chronology.

* Corresponding author.
E-mail addresses: aperttu@ntu.edu.sg (A. Perttu), corentin.caudron@univ-smb.fr (C. Caudron), assink@knmi.nl (J.D. Assink), dmetz@jamstec.go.jp (D. Metz), dtailpied@ntu.edu.sg (D. Tailpied), bperttu@ntu.edu.sg (B. Perttu), hibert@unistra.fr (C. Hibert), DINURF001@e.ntu.edu.sg (D. Nurfiani), christoph.pilger@bgr.de (C. Pilger), muzli@bmkg.go.id (M. Muzli), dfee1@alaska.edu (D. Fee), andersen_oystein@hotmail.com (O.L. Andersen), BTaisne@ntu.edu.sg (B. Taisne).
[1] http://www.oysteinlundandersen.com/.

https://doi.org/10.1016/j.epsl.2020.116268

1. Introduction

Krakatau volcano, located in the Sunda Strait between Sumatra and Java, is well known for its 1883 cataclysmic eruption, collapse, and large tsunamis: destroying coastal towns on Java and Sumatra and killing tens of thousands of people (Simkin and Fiske, 1983). This eruption, created a global pressure wave, recorded on barographs and circled the globe at least four times (Verbeek, 1884; Strachey, 1888). Moreover the eruption was audible five thousand kilometers away in Mauritius. The record of this pressure wave is considered the discovery of infrasound (Evers and Haak, 2010). A new cone, Anak Krakatau, grew on the edge of the 1883 caldera, and has erupted frequently since appearing above sea level in 1927 (Global Volcanism Program, 2013).

Following approximately one year of quiescence, eruptive activity at Anak Krakatau resumed on June 29, 2018, after ten days of elevated seismicity (Global Volcanism Program, 2018; ESDM, 2018a), culminating on December 22, 2018 in a tsunami at ∼21:30 local time (14:30 UTC), killing 437 and injuring ∼31,000 on Java and Sumatra (Syamsidik et al, 2020; Nugroho, 2018a). Post-tsunami the eruption transitioned from Strombolian to Surtseyan and has continued through the time of writing in March 2020. Krakatau has a history of producing tsunamis through various mechanisms, including pyroclastic flows or submarine explosions (1883), underwater explosions (1884, 1928, and 1930), and landslides (1981) (Mutaqin et al., 2019; Ye et al., 2020). Although, the hazard of a tsunami was well known (Giachetti et al., 2012), the collapse was not anticipated in December 2018.

The eruptive activity in December 2018 offers an opportunity to examine the geophysical record of two types of events not well represented in the instrumented record: flank collapse and Surtseyan eruption. Flank collapses at island and submarine volcanoes can generate tsunamis making them a significant hazard and accounting for 20% of volcanic fatalities in the past 400 years (Paris et al., 2014; Grilli et al., 2019). Due to the limited number of detailed observations for flank collapse tsunamigenic events and eruptions, understandings of the associated hazards are based primarily on numerical models (Watt et al., 2019). Such models require accurate emplacement models, something that has historically been lacking.

Here we present an eruption chronology based on official reports, remote geophysical analyses, and eyewitness accounts of Anak Krakatau from December 19 through December 30, 2018. Common with large eruptions at island volcanoes, the local monitoring network was almost totally destroyed (Kristianto et al., 2019) making determining the exact mechanism for tsunami generation difficult. This multi-disciplinary study reveals the eruption chronology of the events leading up to and after the tsunami, helping constrain the tsunami generation, and the subsequent dramatic change in eruption style complementing other recent publications on this event (Walter et al., 2019; Ye et al., 2020; Prata et al., 2020; Grilli et al., 2019; Williams et al., 2019).

1.1. Data and nomenclature

Remote geophysical observations in this study include infrasound, seismic, hydroacoustic, and satellite imagery. Significant signals for each data type are labeled in figures, tables, and text as: Infra for infrasound, Seis for seismic, Photo for photographs and eyewitness accounts, Sat for satellite, Tsu for tide gauge observations, and Hydro for hydroacoustic. We used these datasets to define different phases within the eruption. All times are reported in UTC (local time is UTC+7 hours).

For clarity, we have split this eruption into different phases: Phase 0, the initial phase; Phase 1, the collapse and transition to Surtseyan; Phase 2, renewed activity and growth of the island; and Phase 3, return to intermittent eruptions (Table 1 and Appendix B). We focus on the events within Phase 1, and further subdivided this phase into Phase 1A–E: Phase 1A covers December 22 00:00 through December 22 13:55 before the collapse and tsunami; Phase 1B, the collapse is between December 22 13:55 and 14:00; followed by Phase 1C December 22 14:00–16:55 the propagation and impact of the tsunami along with three discrete eruptive plumes; Phase 1D characterized by sustained activity from December 22 16:55–December 28 05:00; and finally Phase 1E December 28 05:00–December 30, when all observables began to return to background levels as a result of a reduction of activity at the volcano (Table 1).

2. Reported activity

We compiled a timeline of reported activity from official reports via VONA (Albersheim and Guffanti, 2009), VAAC, and press releases. All cloud height measurements are presented as reported and converted to meters in Table A.1. At ∼14:30 a tsunami was reported impacting Java (Phase 1C). Later the heights of the tsunami, measured using tidal gauges along the Javan and Sumatran coast, were reported as between 0.27 m–1.4 m from 14:27–14:35 (Tsu 1-4, Fig. 1, Table 2) (ESDM, 2018b).

In an official press release on December 24, 2018, it was announced that the tsunami was likely caused by a flank collapse of Anak Krakatau (ESDM, 2018b). On December 23, 2018, during local daytime, there was an overflight from Grand Caravan Susi Air, with photos and videos taken by Capt. Mykola and Dicky Adam Sidiq/kumparan (Prata et al., 2020) which confirmed the loss of mass and transition to Surtseyan eruptive activity, reported and shared by Indonesian national disaster agency (BNPB) spokesperson (Nugroho, 2018c, 2018d; AP Archive, 2018). Indonesian agencies preferentially used twitter throughout this event to communicate vital information with the public.

3. Remote geophysical methods

To characterize activity within Phase 1, we analyzed remote geophysical data combined with official alerts. The remote geophysical observations include infrasound, seismic, hydroacoustic (Fig. 1), and satellite observations. Although local, real-time sensor networks are the most effective for volcano monitoring, it is important to improve analysis via remote technologies, as many volcanoes are not equipped with local real-time monitoring (e.g. Coombs et al., 2018).

3.1. Infrasound

Phase 1 was recorded by the International Monitoring System (IMS), and other regional infrasound stations. Infrasound was recorded as individual detections for Phase 0, and sustained detections for Phase 2.

We analyzed infrasound signals using several data processing approaches: array processing, spectral analysis, and beamforming (Fig. 2). The clearest signals were detected on I06AU (Cocos Island), ∼1160 km to the SW of the volcano (Fig. 1). Signals were also recorded on the Singapore Array (SING), and Marapi Volcano Infrasound Network (MARP) on Sumatra. In addition to the sustained infrasound detections observed at I06AU throughout Phase 1, the collapse (onset of Phase 1B) produced a relatively high-amplitude, low-frequency signal at I06AU, SING and MARP (Fig. 2 and Fig. A.3).

During Phase 1A (00:00–13:50 December 22, 2018), circa 06:30 at station I06AU, array processing detections changed from isolated to sustained detections (Infra1). Considering distance, and average

Table 1
Definitions of the Phases defined for use in the text, along with specific significant signals. Infra derives from signals recorded via infrasound, Seis from the seismic data, Sat from the satellite data, and Tsu from the measurements of the tsunami from the tide gauges. Photo is related to the observations by eyewitnesses.

Phase	Date/Time UTC (2018-2020)	Description of Volcanic Activity	Specific signals
Phase 0	June 18– December 21	Initial activity, characterized by Strombolian explosions with a range of intensities, ash plumes less than 5 km, and lava flows	
Phase 1	December 22– December 30	Collapse and transition to explosive and Surtseyan style eruptions with high level plumes over 10 km	
Phase 1A	December 22, 00:00–13:50	Intense Strombolian activity, possible lava flow on SW flank, ejected incandescent material reaching the sea	Infra1; Infra2; Seis1a & 1b; Seis2; Photo1; Photo2; Photo3; Sat2
Phase 1B	December 22, 13:50–14:00	Collapse of Anak Krakatau cone and generation of tsunami	Infra3; Infra 3a & 3b; Seis3
Phase 1C	December 22, 14:00–16:55	Propagation and impact of tsunami and three phreatomagmatic eruptions, directly after collapse at 13:55, 15:25, and 15:55	Photo5; Seis4; Seis6; Sat4; Sat5; Sat6; Tsu1; Tsu2; Tsu3; Tsu4
Phase 1D	December 22, 16:55– December 28, 05:05	Sustained high level plume with intermittent pulsing and SO_2 detected	Infra4; Sat6; Sat7; Sat8; Sat9; Seis6
Phase 1E	December 28– December 30	No sustained plume from satellite and ramp down in geophysical observations	
Phase 2	January 2019	After a pause another period of high level plumes and the rebuilding of the island	
Phase 3	February 2019 – time of writing	Sporadic eruptions	

Table 2
Geophysical observations of tsunami and collapse signal of Anak Krakatau, on December 22, 2018.

Station	Technology	Range (km)	Back-azimuth (deg)	Arrival Time of Tsunami	Measured Height of Tsunami
Marina Jambu	Tide gauge	45		14:27	1.4 m
Stasiun Panjang station	Tide gauge	70		14:27	0.36 m
Kota Agung Station	Tide gauge	110		14:35	0.31 m
Banten Station	Tide gauge	55		14:40	0.27 m
				Arrival time of Collapse Signal	
I06AU	Infrasound	1156	55	15:01:15	Detected
I07AU	Infrasound	3480	292		No detection
I52GB	Infrasound	3643	90		No detection
SING	Infrasound	842	168	14:44	Detected
MARP	Infrasound	839	140	14:42	Detected
IA-CGJI	Seismic	64		13:56	Detected
GE-JAGI	Seismic	998		14:01:40	Detected (farthest)

celerity of 0.3 km/s, we estimate Anak Krakatau became acoustically active circa 05:30. The signal was coherent between 0.8 to ∼3 Hz; by 07:08 the lowest frequency dropped to ∼0.6 Hz, then to 0.5 Hz by 07:50. From 08:00 through 13:00, the signal-to-noise (Smart and Flinn, 1971) power level increases; observations consist of a sustained signal interspersed with short-lived transients (Fig. 2c). Around 14:34, we noted an infrasound coherence gap from the direction of Anak Krakatau (Infra2). The gap only lasts about 5 min, after which the sustained signal resumes (Fig. A.2) and is further discussed in section 5.1.1.

At 15:01:15, we detected a large amplitude, low frequency signal (Infra3), with a dominant frequency of 0.2 Hz, and a peak-to-peak amplitude of 6 Pa (Figure 2). We used the parabolic equation (NCPA PAPE, see Waxler et al., 2017; Waxler and Assink, 2019) and ray-tracing (Waxler et al., 2017; Waxler and Assink, 2019) to model the acoustic propagation path, ducting, expected travel time, and celerity. The result (Fig. A.1) for I06AU is a stratospheric arrival with a celerity of 0.290 km/s originating at 13:54:51 at the volcano, which is consistent with a seismic signal recorded ∼13:55 at the volcano and tsunami generation (see section 3.2). This signal is bracketed by two small amplitude transients with similar frequency content, ∼14:59 (Infra3a) and 15:02:45 (Infra3b). After this sequence we observed a significant drop in frequency content, indicating that the coherency had shifted to 0.1–2.0 Hz (Figs. 2a, b). After 22:00, the station intermittently detected low frequencies down to 0.02 Hz. The detectability of signals in the 0.01–0.1 Hz band is strongly dependent on the wind noise levels near the array, with higher noise during local daytime (Christie and Cam-

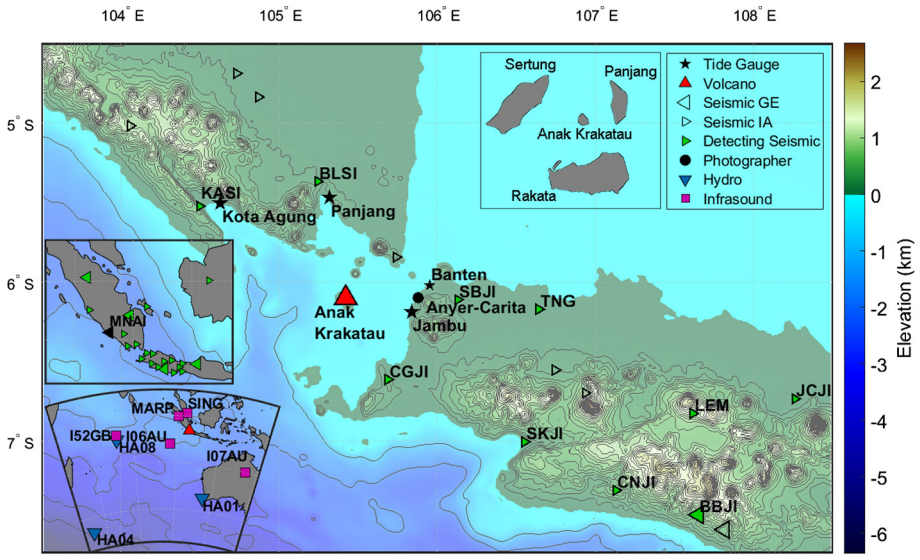

Fig. 1. Location Map. Relative location of Anak Krakatau cone (red triangle) and the locations mentioned within the text. Seismic stations symbols are triangles: GEOFON network (GE) represented with a relatively larger symbol and pointing to the left, while the BMKG network (IA) triangles are pointing to the right. Seismic stations detecting the signal of Phase 1B are green (GE-BBJI, GE-BKNI, GE-JAGI, GE-MNAI, GE-PMBI, GE-SMRI, IA-BLSI, IA-CGJI, IA-CMJI, IA-CNJI, IA-CTJI, IA-JCJI, IA-KASI, IA-KPJI, IA-LEM, IA-MDSI, IA-MKBI, IA-NGI, IA-PPBI, IA-SBJI, IA-SCJI, IA-SKJI, IA-STKI, IA-TNG), and non-detecting stations are red. Hydroacoustic station symbols are blue triangles. Infrasound station symbols are purple squares. Tide gauges that reported tsunami heights are star symbols. Tsunami heights measured from the following stations were: Marina Jambu, 1.4 m; Banten Station, 0.27 m; Kota Agung Station, 0.31 m; and Panjang Port, 0.36 m. The observation location of photographer Øystein Lund Andersen, Anyer-Carita, is a diamond symbol. (For interpretation of the colors in the figure(s), the reader is referred to the web version of this article.)

pus, 2010). This is consistent with local wind speed measurements, (Fig. 2b).

Phase 1A, Phase 1B, and Phase 1C were detected by only I06AU from the regional IMS infrasound network. During this time at I52GB array processing results are dominated by coherent microbaroms (non-linear interactions of ocean and atmosphere) but began to pick up detections on the next day (Fig. 1, Table 2). Sporadically throughout Phase 1D, detections were reported at I04AU, I07AU, I39PW, and I40PG, in the Reviewed Event Bulletins (REB), published by the Comprehensive Nuclear-Test-Ban Treaty Organization (CTBTO). A frequency and range dependent atmospheric attenuation modeling technique was used to compare the detection pattern with the expected pattern (see Appendix B, Section 5.2, and Fig. A.1). The detection at I06AU is expected, and non-detections at I07AU, I39PW, and I40PG of Phase 1B are expected, however these results indicate that I52GB should have detected this signal given the amplitude recorded at I06AU.

In addition to the IMS stations within the region, there are also infrasound sensors located within Singapore (SING), and around Marapi volcano (MARP), both of which are approximately 840 km from Anak Krakatau (Fig. 1, Table 2). Walter et al. (2019) also note that the airwave associated with Infra3 was observed on several regional seismic stations. Phase 1A (Infra3) was recorded at 14:42–14:47 as coherent infrasound in the 0.05–0.5 Hz frequency band (Fig. A.3). The recorded peak to peak amplitude at SING and MARP are approximately 0.4 Pa, which is significantly smaller than the observed arrival at I06AU. Our observations approximate first-order simulations of the infrasound propagation in terms of detectability, but fail to explain the discrepancy of ∼30 dB between expected and recorded amplitude at MARP and SING (Fig. A.1).

3.2. Seismic

We analyzed seismic data from stations located up to 600 km from the volcano (GEOFON Data Centre, 1993; BMKG Data Centre, 2015). The sequence observed at the nearest seismic station, CGJI, includes four clearly identified seismic signals (Fig. 3).

Firstly, we observed two high-frequency emergent signals (10–20 Hz, Fig. 3d, g) between 12:50 and 13:00 (Seis1a and 1b, respectively, Phase 1A). Their emergent waveform, high-frequency content (>10 Hz), duration of tens of seconds, and lack of clear wave polarization are consistent with landslide signals. Fast-moving aerial landslides generate high-frequency waves, generated by granular interactions at the base of, and within the bulk of, the moving masses (e.g. Farin et al., 2015, 2019; Hibert et al., 2015, 2017; Bachelet et al., 2018); for smaller events they are only recorded close to the source as they attenuate more rapidly than the lower frequency waves (>10–30 s), which are only generated by the largest events (e.g. Allstadt, 2013; Ekström and Stark, 2013; Hibert et al., 2014, 2015). Second, we observed a short, relatively high-frequency (1–10 Hz, Fig. 3c, f, Seis2, Phase 1B) signal at 13:54 only at CGJI, two minutes before a larger amplitude, broadband seismic signal (∼13:56 at the stations around the volcano, Seis3, Phase 1B). This signal Seis2 is discussed in detail in section 5.2.

We observed this larger amplitude, broadband seismic signal, Seis3, across the GFZ (GE) and BMKG (IA) seismic networks (up to West Sumatra and East Java), coincident with the collapse (Fig. 3f), and registering as a M_w5.1 at 13:55:48.7 in the GEOFON Program automated system (GEOFON Data, 2018). The waveform is complex, with emergent low-frequency oscillation (<1 Hz) followed by sustained high-frequency energy above 1 Hz, probably reflecting the superposition of different sources, such as landslides and explosions. Particle motion of signals filtered between 10–130 s (Fig. A.4) show energy preferentially radiated on horizontal components, with polarizations perpendicular to the azimuth between stations and the localization of source. This suggests a signal dominated by Love waves, consistent with a gravitational source and west/south-west mass motion (e.g. Kanamori and Given, 1982). This is in agreement with the results of Walter et al. (2019) whose waveform inversion results give a focal mechanism with a significant non-double couple component and oriented SW at 222°. Ye et al. (2020) calculated a slide volume from the seismic data of ∼0.15–0.2 km^3. Post-collapse, high-frequency energy (1–10 Hz) remained elevated, and a 40 min duration, large, low frequency signal was recorded (0.01–0.1 Hz, Fig. 3b, e, Seis4, Phase 1B). We

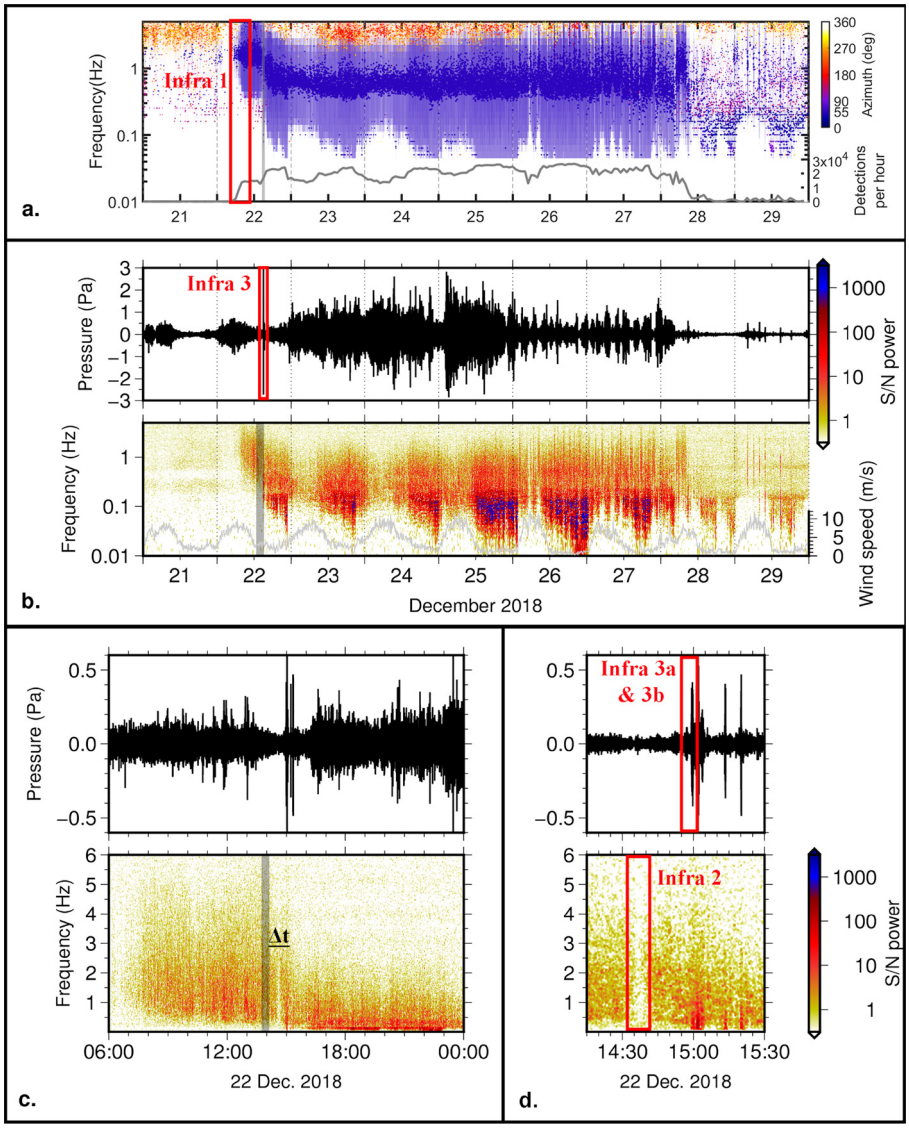

Fig. 2. Infrasound analysis on I06AU during the first eruption phase of Anak Krakatau from December 21–29, 2018. The frames show the measured array processing results, pressure, and spectrogram on the beam towards Anak Krakatau. (a) The array processing results from I06AU. Array processing was performed with the Progressive Multi-Channel Correlation (PMCC, Cansi, 1995), using nth octave bands and window lengths scaled with frequency (Garces, 2013), and filtered for detections within 10 degrees of the calculated back-azimuth of the volcano from each array. The range of frequency for each detection family is plotted colored by the back-azimuth, and the mean frequency of the family is plotted as a dot. Below is the detection rate of pixels per hour within 10 degrees of the known back-azimuth of the volcano. Infra1 depicts the sustained array processing results that began early on the 22nd. (b) Pressure record of I06AU beamformed towards Anak Krakatau, and coherence spectrogram with wind speed. The complete sequence of arrivals, with the main eruption on December 22 and the transition from Strombolian to Surtseyan activity, showing that the signal is most coherent between 0.01–0.1 Hz in the days following the collapse event. A logarithmic frequency axis is used to outline the tonal characteristics in this part of the spectrum. The low frequency signal Infra3 is associated to Phase 1B. The detectability of these low-frequency signals is hampered during high wind conditions. Above ~0.1 Hz, individual pulses are outlined with a particularly high signal power on December 26–27. (c) The zoom in on December 22 shows the characteristics of coherent infrasound that precedes the collapse event (indicated with a vertical bar). This signal is a combination of quasi-continuous noise and transient signals and is mostly coherent between 0.5–4.0 Hz. The offset between the collapse time of the event and the signal being recorded at I06AU is plotted and is consistent with a stratospheric arrival. (d) The signal is sustained until the signals associated with the main eruption arrive at I06AU, except for a moment of quiescence between 14:35 and 14:40 (Infra2). The main eruption is observed at I06AU around 15:00; the associated signal has a dominant frequency around 0.2 Hz and has a duration of approximately five minutes. Infra3a and 3b are short signals that occurred prior to the collapse signal.

ascribe this signal to the tsunami hitting the coast, consistent with timings reported in Grilli et al. (2019). A magnitude 6.0 earthquake occurred in the Vanuatu region, at 14:24, and was globally recorded (Fig. 3a, Seis5, Phase 1B). Finally, after this sequence, spectral lines can be observed when computing spectrograms with time windows above 30 s at several stations, up to 371 km from Krakatau, from directly after the collapse until December 27, 2018 (Fig. A.5, Seis6, Phases 1C & 1D). By lowering the window length below 30 s, these spectral lines disappear in the spectrograms, suggesting the existence of repeating events at the source, rather than seismic tremor.

3.3. Hydroacoustic

Hydroacoustic data have been used to remotely detect and study activity at both partially and fully submerged volcanoes, e.g. during the recent eruptions of Anatahan and Ahyi volcano in the Mariana Arc (Dziak et al., 2005; Metz and Grevemeyer, 2018). However, records of acoustic measurements made by three IMS hydrophone stations, located at Cape Leeuwin (HA01), Crozet Islands (HA04), and Diego Garcia (HA08, cf. Fig. 1), show no discrete clusters of arrivals that could be interpreted as long-range detections

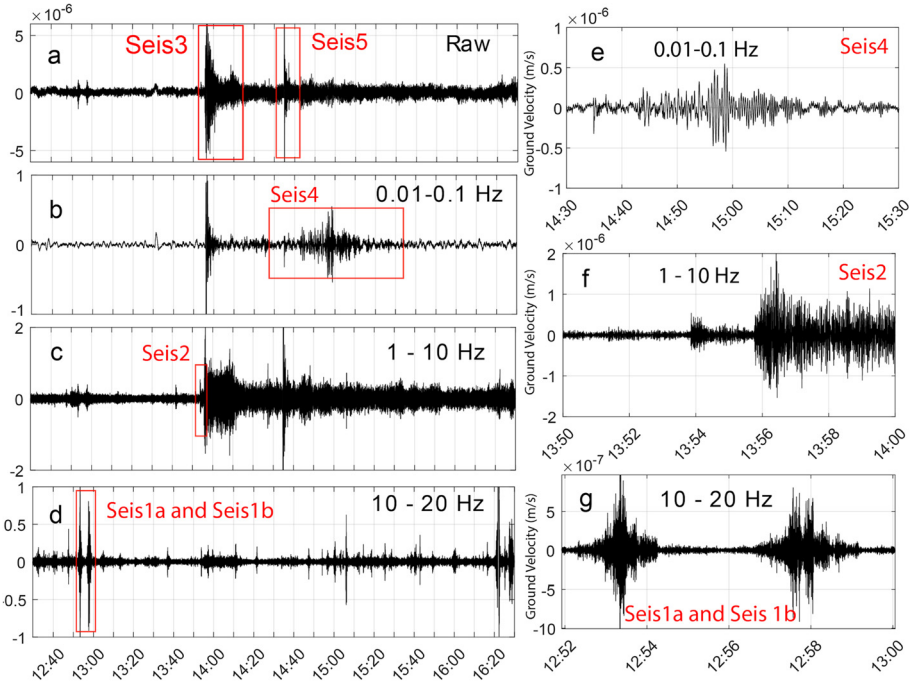

Fig. 3. Seismic observations from station IA-CGJI located ~64 km from Anak Krakatau on Java (Fig. 1) plotted within different frequency bands to highlight different signals. Seis3 (a and f) is the large amplitude signal consistent with the largest mass loss at Anak Krakatau. Seis2 is a small amplitude signal 2 min prior to Seis3 (c and d) and interpreted to be a small landslide. Seis1a and 1b (g) are characteristic of two landslides consistent with Anak Krakatau around 12:52 and 12:57 UTC. Seis4 (e) is a signal characteristic of a tsunami hitting the coast. Seis5 (a) is a teleseismic arrival from an unrelated earthquake in Vanuatu.

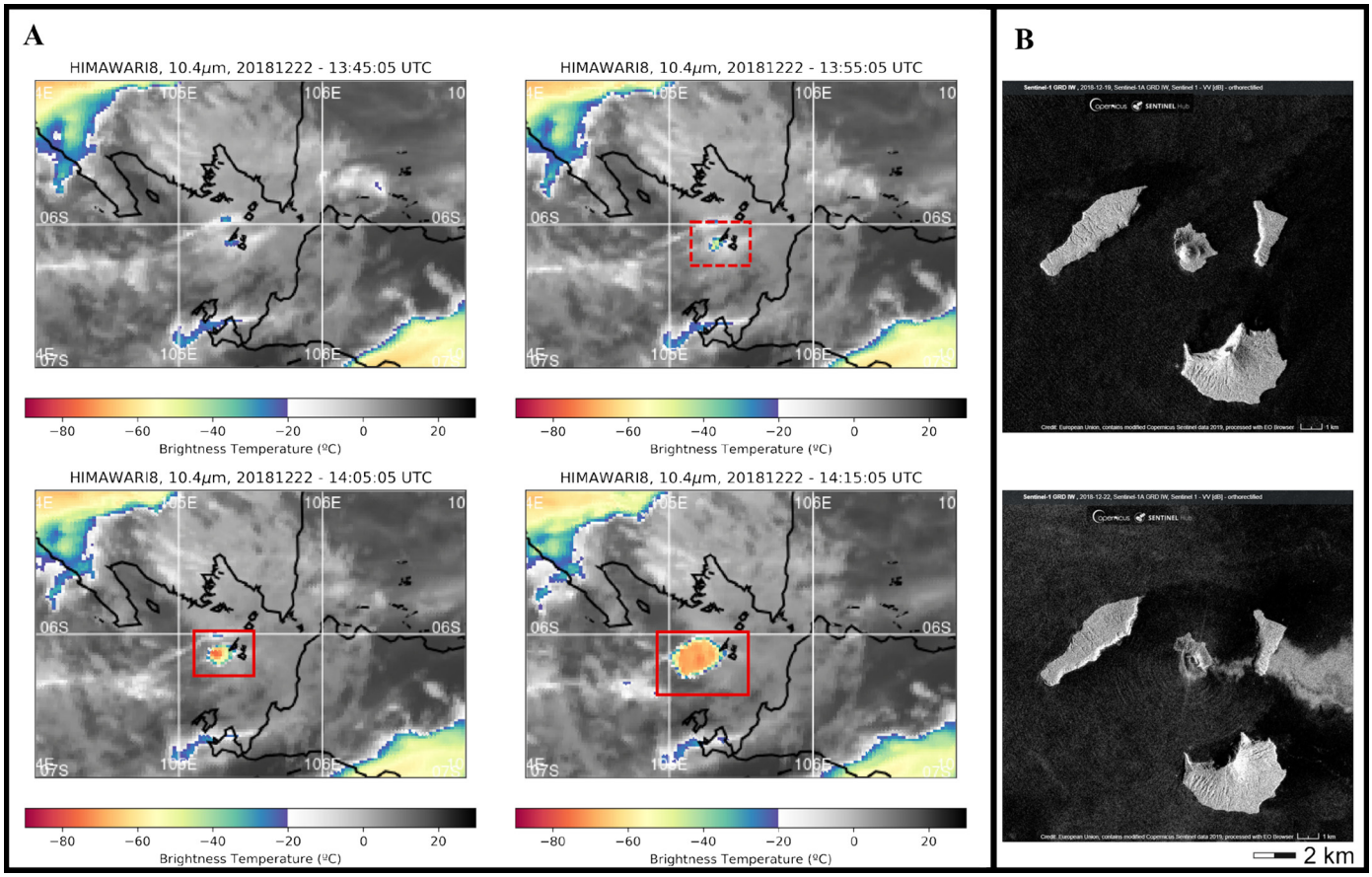

Fig. 4. Satellite observations on December 22 of Anak Krakatau. A is four scenes from Himawari-8 10.4 μm channel on December 22 from 13:45–14:15 UTC. The color bar is plotted in terms of brightness temperature. The dotted red rectangle in scene 13:55 UTC is the potential first detection of the plume visible (in red rectangles) in scene 14:05 UTC and 14:15 UTC. B is the two Sentinel-1A overpasses that bracket the tsunami: the first (top, ascending) on December 19, 11:23 UTC, and the second (bottom, descending) on December 22, 22:33 UTC.

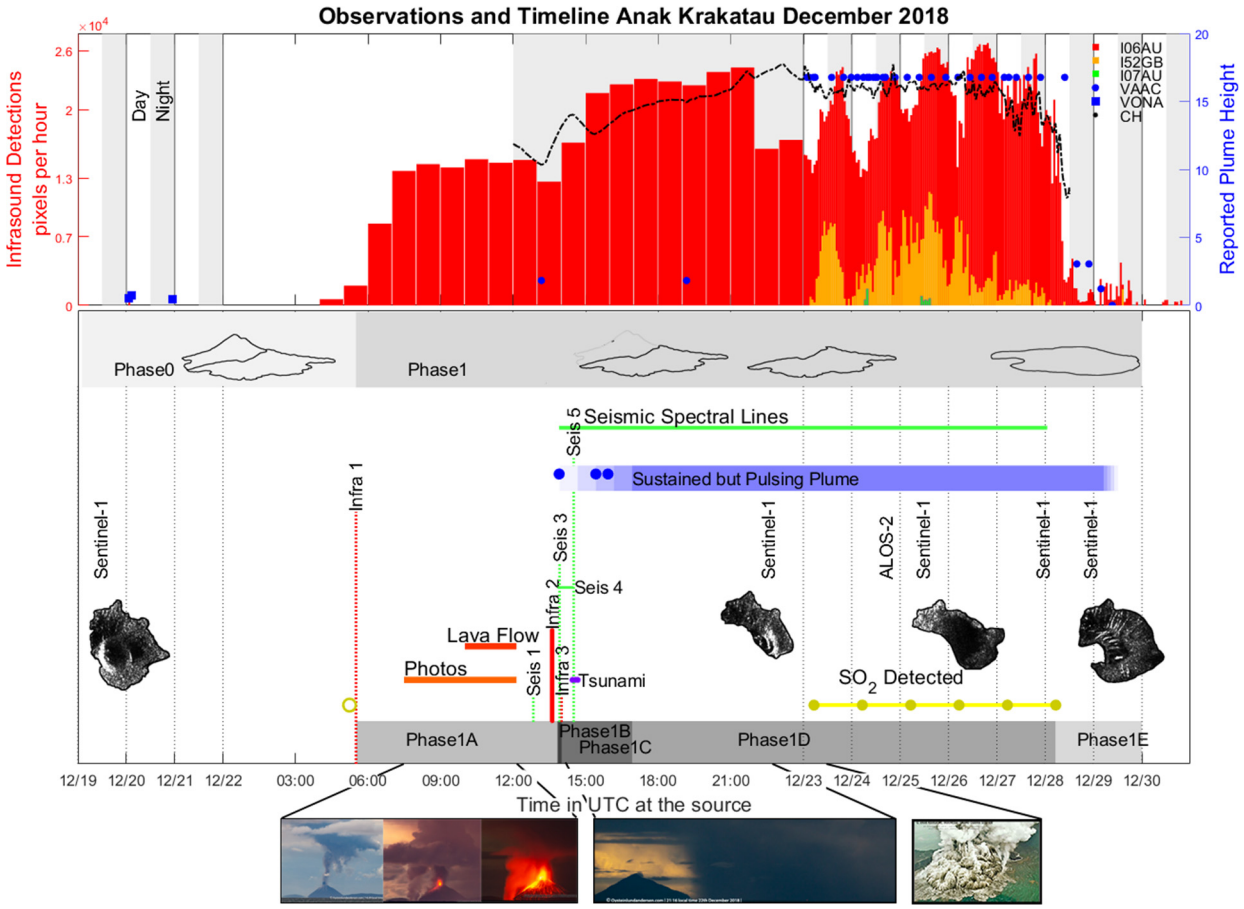

Fig. 5. Timeline of activity at Anak Krakatau in December. In the top panel the observations from the VONA and VAAC alerts are plotted in blue, the cloud heights (CH) from Himawari-8 from Prata et al. (2020) are plotted in black, and the infrasound detections are plotted with a time offset corrected for time at the volcano for I06AU (red), I52GB (orange), and I07AU (green). Grey boxes are included to depict the different phases of the eruption through time. The initial phase, Phase 0 (12/19–05:30 12/22) is characterized by intermittent Strombolian, Phase 1A is characterized by a transition to intense Strombolian (12/22 05:30–12/22 13:55), Phase 1B (13:55–14:00) is when the tsunami was generated, Phase 1C (14:00–16:55) is characterized by three phreatomagmatic eruptions after the collapse, Phase 1D (12/22 16:55–12/28) is characterized by sustained Surtseyan activity, and finally Phase 1E is characterized by ramping down of activity and geophysical observations. The time axis has been stretched on December 22nd in order to include all the signals in the lower panel. Above this is a cartoon based on photographs of the morphology of the volcano through time. The outlines of the island of Anak Krakatau from both Sentinel-1 (S) (modified Copernicus Sentinel Data, 2018) and ALOS-2 (A) (ALOS-2 Project, 2018) are also included for the passes on 12/19 11:23 (S), 12/22 22:33 (S), 12/24 17:13 (A), 12/25 11:22 (S), 12/27 22:41 (S) and 12/28 22:33 (S). Photographs of activity are also included and the time period where they were taken documenting the activity is highlighted with a blue line (Figs. A.7–A.11). Also included is an example of how the volcano appeared obscured with ash after the collapse (Fig. A.12) and a photo from the overflight on 12/23 showing Surtseyan activity (Nugroho, 2018b). The time period interpreted to be a lava flow from the photos is noted in red. Significant signals in infrasound and seismic data are noted with vertical lines colored for technology: with green for seismic, and red for infrasound. The horizontal purple line is the time between the generation of the tsunami and the initial impacts on the Sunda Strait coast. The plumes detected after the collapse are noted with a blue dot, and the period of sustained but pulsing activity is noted by a blue bar. The period of seismic spectral lines is noted in green. The period of detected SO_2 is noted in yellow, with the time of the specific measurements. (For interpretation of the colors in the figure, the reader is referred to the web version of this article.)

of activity at Anak Krakatau during the December 2018 episode (Fig. A.6, Appendix B).

3.4. Satellite

Anak Krakatau is within the field of view of the satellite Himawari-8 (Himawari Cloud Dataset, 2015; Bessho et al., 2016), however for most of the day on December 22 meteorological clouds obscured the view of the volcano. From satellite data, the cloud height throughout the local day ranged from ~5000 m to ~12,000 m, with higher meteorological clouds dissipating in the hours prior to the tsunami generation, thus any plumes produced below this level would not have been visible from satellite. We derived timing from Himawari-8 header data, which indicated that the section of the scenes covering Anak Krakatau were captured ~4–5 min after the scene name time (e.g. 13:00 scene captured at between 13:04–13:05) and is the time used to refer to the individual scenes captured. While activity associated with the ~05:30 initiation of infrasound detections is obscured from satellite, we know from the activity reports (VONA/VAAC) and local observers, that a plume was visible from the ground. There is a clear volcanic plume within the 13:55 Himawari-8 scene, persisting for several scenes (Fig. 4). This plume ranges from ~12–16 km above sea level with duration circa 60 min based on satellite data. There is a second pulse in the 15:25 scene (Sat4) with duration circa 20 min, and a third in the 15:55 scene (Sat5) with duration circa 50 min. After the 16:55 scene (Sat6) it appears that the volcano entered a period of sustained eruption with fluctuating intensity until 05:05 December 28 (Sat9).

The SO_2 cloud was observed by the TROPOMI instrument on the Sentinel-5 satellite starting on December 23 in the 05:14 observation, and drifted towards the SW (Prata et al., 2020). The previous overpass was around the same time on December 22, and therefore there is no measurement of the presence of SO_2 from this satellite between the collapse and the December 23 overpass. SO_2 emissions continued to be observed until the December 28 05:20 scene (Gouhier and Paris, 2019; Prata et al., 2020). Radar images from Sentinel-1 and ALOS-2 (ALOS-2 Project, 2018) track evolution of the island throughout this period, from December 22–29, and

show the change in island morphology after the collapse on December 22 (Fig. 4 and 5).

4. Eyewitness observations

Another data source comes from two types of eyewitness accounts: first, TV interviews of several surviving fishermen who witnessed the entire sequence while fishing close to Anak Krakatau on the 22nd of December; second, observations of a co-author of this paper (photographer Andersen Øystein), who was documenting the eruption from Anyer-Carita on the Java coast about 47 km from Anak Krakatau.

According to one of the surviving fishermen, Puji (Lampung TV, 2018), on December 22 the volcano was not exhibiting an unusual level of activity, which was why that evening ∼15–18 fishermen were in the area. He estimated that his boat was approximately 700 m from Anak Krakatau. He stated that he observed an eruption on "west side" of the volcano, saw the volcano "split into two", and "lahar went everywhere" (which could be referring to pyroclastic activity, as lahar has the same translation as lava). The split was followed by three tsunami waves, of which the 3rd was the most powerful, and estimated to be about 12 m high. Although Anak Krakatau was hidden from view after the collapse he reported two additional collapses, with the third on the "east" side (these could also be two large explosions). Reconstructing the chronology based on Puji's account, the eruption began with flank activity, followed by a collapse of the central part of the island, triggering the tsunami. Two additional collapses ensued, with the time between the first and second collapse reported as being longer than that between the second and third. A second fisherman, Roni Herliansyan (Lampung TV, 2019), added that on the 22nd activity at Anak Krakatau increased relative to the previous two days: about 12:00 they decided it was too dangerous to return to the island where they had been camping, and about 13:00 he observed lightning within the eruption. A third fisherman, Ari Agus (TvOneNews, 2018), stated that about 14:00 Anak Krakatau ejected incandescent lava three times before collapsing. All three interviews include details about the tsunami within the islands surrounding Anak Krakatau (Fig. 1). In addition to citing the number of waves and the height, Puji also stated that the water smelled of sulfur, was hot, and had a cloudy color like milk coffee. Roni Herliansyah, did not directly observe the collapse but stated that there were 4 waves, and that he saw Sertung Island covered by one of the tsunami waves which he estimated to be 25 m. He also stated that after a large wave the water receded and he was able to "run" before being hit by additional waves. Ari Agus stated that his group was hit by three waves, and estimated the waves to be between 30–40 m high. All interviews were conducted in Indonesian and have been translated with some interpretation of the language in terms of proper volcanologic terminology for types of activity. All interviews agree that the first wave was not the largest and while the number differs between 3 and 4 the last is always cited as the largest.

Observations recorded from Java by co-author Øystein L. Andersen, began on December 22 about 07:30 UTC, and described a summit plume at Anak Krakatau which extended into the basal cloud cover (Photo1, Fig. A.7). Eruptions were audible every 10 to 30 s. At 10:00 volcanic activity increased (Photo2), with a higher plume and more frequent sounds. Approximately 10:30 an additional white plume appeared on the southern flank of Anak Krakatau (Photo3, Fig. A.8). By 11:00, the white plume had migrated down the flank towards the shoreline, and became increasingly vigorous. By 11:20 ambient light was reduced enough for lava fountaining to be observable (Fig. A.9). The peak in the activity occurred ∼11:30, with stronger eruption sounds, with both plumes still visible, but no visible incandescence associated with the second plume (Fig. A.10). At 11:55, incandescent ballistics were observed to reach the shoreline on all visible sides of Anak Krakatau, with higher incidence on the south flank. At 12:05 incandescence illuminated the second plume (Fig. A.11). From 12:08 to 14:05 there are no reported visual observations, and between 13:30 and 14:00 audible eruption sounds appeared to have ceased (Photo4). At 14:15 the entirety of Anak Krakatau Island was obscured by a dark cloud, while Rakata Island, only 3 km to the southeast, was clearly visible (Photo5, Fig. A.12). At 14:27 the tsunami began impacting the observation area. (Please see http://www.oysteinlundandersen.com/krakatau-volcano-witnessing-the-eruption-tsunami-22december2018, appendix C for more details.)

5. Discussion

Combining the reported activity with the infrasound (Fig. 2), seismic (Fig. 3), hydroacoustic (A.6), satellite (Fig. 4), and eyewitness observations (Fig. A.7-12) allows us to build a detailed chronology on December 22, and continuing through the end of this phase (Fig. 5).

5.1. Pre-tsunami

Before the tsunami, activity, while intense, was similar to that seen earlier in the eruption (September–October, 2018 Fig. A.13). The transition from sporadic eruptions to continuous Strombolian activity was documented by relatively high-frequency infrasound beginning ∼05:30. In order to determine if the infrasound in Phase 1A is consistent with previous levels of activity or if it could be considered anomalous, it was compared to infrasound observations from a previous study in 1999 (Kristianto, 1999) and a period of heightened activity in October 2018. The amplitudes reported from the previous study are consistent with the pre-collapse amplitudes at I06AU, and the character of the detections in October 2018 are similar to the detections in early December 22 (Appendix B). The eyewitness accounts both mentioned a crescendo in activity between 10:00–12:00, around the time that a possible lava flow was observed from Java (secondary white plume in photos), consistent with an increase in power level at I06AU. The seismic signals Seis1a and Seis1b (12:50 and 13:00) are consistent with landslides, and the multiple peaks in the waveform signal are typical of a landslide encountering topographical barriers (Hibert et al., 2014, Appendix B). The sharp coda decay is unusual, and could result from the descending mass flow rapidly reaching the sea decoupled from the land surface. This signal was only observed at station IA-CGJI, the closest seismic station to the volcano (Fig. 1) and local seismic data would be required to definitely determine the source of these signals. Yet this signal indicates potential destabilization of the edifice prior to the main collapse event (Phase 1B) (Appendix B).

5.1.1. Momentary quiescence

There is an approximately 5 min long pause in the Anak Krakatau infrasound detections at I06AU that occurs in the 30 min leading up to the collapse (Infra2) (Fig. 3). However, at this distance, ∼1150 km, the duration of this gap at the source could be longer due to uncertainties in propagation modeling. This gap is likely due to source processes, as there is no increase in local station noise or another signal interfering in that time period (Fig. A.2). The timing of the infrasound observation coincides with the observation of a lack of audible eruption sounds. However, there are no direct visual or satellite observations during this timeframe due to a meteorologic cloud shielding the volcano. Additionally, it is possible that the lack of audible eruption sounds reported from 13:30 to 14:00 could be due to the lowering of frequency out

of the audible range. There are also reports of a decrease in infrasound prior to eruptions attributed to sealing processes (Yokoo et al., 2013). Similar observations of precursory seismic quiescence have been reported preceding both phreatic and magmatic explosions (Newhall and Endo, 1987; Hotovec et al., 2013; Roman et al., 2016), and have been interpreted as sealing of gas pathways or formation of a plug (Appendix B).

5.2. Collapse and tsunami

Phase 1B, the collapse is bracketed by two overpasses from Sentinel-1 on December 19 and at 22:33 on December 22, 2018, confirming a dramatic change in morphology (Babu and Kumar, 2019; Gouhier and Paris, 2019; Grilli et al., 2019; Williams et al., 2019). Up until 12:08 (∼2 hours prior to the collapse signal) the morphology of the island was unchanged as confirmed by photographic observations (Fig. A.7–A.11). Around 10 min after the collapse (assuming a ∼13:55 time) Anak Krakatau was obscured from view (Fig. A.12) while the neighboring island of Rakata was visible. Between this time and the overpass of the Sentinel-1 at 22:33, there was no direct observation of the island of Anak Krakatau, except by the fishermen.

The most likely scenario is one landslide into the sea on the SW side of the island, which was recorded both seismically (Seis3) and infrasonically (Infra3). There is no evidence for an unusually large explosion preceding the collapse. However, prior to the collapse there was heightened activity as well as flank activity a second small white plume recorded in the photographs taken from Java. This possible lava flow could be what the fishermen were referring to when they described an eruption “on the side”.

The small signals analyzed a few minutes before the collapse in both seismic (Seis2) and infrasound (Infra3a) data are not consistent with a large eruption triggering a collapse (Fig. 5). Evidence from the seismic recording at station IA-CGJI indicates this signal was likely generated by a small slide that reached the sea (Appendix B). There was no observed explosion signal recorded at MARP and SING prior to the collapse signal. The main signal from the collapse Infra3 recorded at I06AU corresponds with stratospheric arrival from a ray with 6 bounces and a calculated celerity of 0.2902 km/s (Fig. A.1). Additionally there is a waveguide that can be modeled with 5 bounces instead of 6 with a higher celerity and lower amplitude. This would correspond to the signal Infra3a recorded at 14:49:00. It is also probable there are rays with 7 bounces accounting for the additional arrival Infra3b (Fig. A.15). Multiple arrivals from the same source signal were seen and well documented for the Buncefield explosions in 2005 (Ceranna et al., 2009). The multiple signals were not clearly observed at SING and MARP. The duct is more stable towards MARP but there is no evidence for multipathing at this station. Due to the multipathing in the ray tracing results and observed at I06AU, combined with the lack of multiple signals at SING and MARP, Infra3a, Infra3 and Infra3b are interpreted as due to the same source signal: the collapse of Anak Krakatau at 13:55:48.7 (GEOFON data, 2018) and are therefore not consistent with an explosion prior to this collapse as proposed by Walter et al. (2019). The difference between infrasonic and seismic origin time is only 1.4%, or 58 s over 66.5 min. This difference of ∼1 min is well within errors for infrasound propagation, and both are highly likely to be generated by the same event. However, it is also likely that the seismic signal is generated at the failure plane at the base of the slide, and the infrasound is generated from the movement and collapse of the Anak Krakatau cone itself, which would also be consistent with the eyewitness report that the volcano “split in two” (Section 4).

Infrasound generated from mass movements is not well understood, but one theory is that the mass acts like a piston and pushes the atmosphere out of the way, acting as a dipole (Allstadt et al., 2018). Dipole radiation patterns in infrasound have been studied in the context of volcanic explosions, and Matoza et al. (2013) illustrate that the amplitude of the infrasound signal is dependent on the angle from the direction of the dipole. There is a strong radiation pattern in the infrasound signal amplitude from the collapse. The atmospheric attenuation modeling completed for the event assumes a monopole, or isotropic, radiation pattern from the source and fails to explain the difference in amplitude observed in Singapore (SING) and at Marapi Volcano (MARP) given the amplitude at I06AU. The modeling suggests approximately the same amplitude is expected between these stations. Additionally, given the amplitude at I06AU, the amplitude expected for I52GB is above the microbarom noise level, however there is no clear detection. Therefore it is possible that the collapse follows the reasoning in Allstadt et al. (2018) and acts as a dipole. I06AU is in fact located to the SW of Anak Krakatau, the direction of the collapse and a dipole would explain the relative amplitudes observed. Further propagation modeling (Appendix B) even when considering extreme uncertainties (up to 10% or +/− 30 m/s wind speed) in the atmospheric specifications are not able to explain the discrepancy in amplitude.

Based on the eyewitness report of the volcano being “split in two” (Section 4), as well as the strong infrasound detections, the most likely scenario for generating the tsunami is a large collapse that was at least in part subaerial. Walter et al. (2019) note that they observed deformation of the island with InSAR analysis before the collapse in a pattern consistent with a progressively sliding flank with a deep decollement plane at ∼0.85 km depth and the flank sliding to the SW. Recent modeling of the flank collapse by Grilli et al. (2019), based on the tsunami data, suggests that the cone of Anak Krakatau failed en mass to the SW, and therefore accounts for the majority of the missing portion of the edifice seen in the Sentinel-1 overpass 8 hours later. Their results indicate a volume of 0.22–0.3 km^3 with a preferred value of 0.27 km^3 and total run-up on the local islands consistent with the fisherman’s accounts (see section 4). The fishermen reported a variety of number and size of waves, and while there is room for error in their estimation of heights, due to the complexities of the propagation of the tsunami around the local topography it is plausible that different locations around the island experienced different numbers and size of waves. While Grilli et al. (2019) state that their simulation does indicate multiple waves hitting the coast with the later waves being the largest they do not explicitly mention this for the area immediately around the volcano. Several additional studies base their morphology change estimates on satellite images and differ on whether the majority of the post-1980 cone was involved (Gouhier and Paris, 2019; Grilli et al., 2019; Walter et al., 2019) or only part of the cone (Williams et al., 2019). This difference is reflected in the range of volume estimates from ∼0.09 km^3–0.1 km^3 (Gouhier and Paris, 2019; Williams et al., 2019; Walter et al., 2019) to 0.22–0.3 km^3 (Grilli et al., 2019).

5.3. Sustained activity

5.3.1. Infrasound frequency drop

There is a clear change in the frequency content of the infrasound signal recorded at I06AU after the collapse signal (Fig. 2). This can be interpreted as a change from the regular subaerial Strombolian activity before the collapse to more Surtseyan activity as seawater infiltrated the vent, evidenced by the change in the edifice seen in Sentinel-1 data. This change in activity changed the acoustic source, explaining the change in frequency content. A similar, dramatic change in infrasound frequency content was observed for shallow submarine (Surtseyan) activity at Bogoslof volcano, Alaska (Fee et al., 2020; Lyons et al., 2019, 2020). This change in frequency is temporally consistent with seismic spectral

banding, indicating Surtseyan eruptions began immediately after the collapse.

5.3.2. Seismic spectral lines

Clear lines appear in the spectrograms immediately after the onset of the eruption. By lowering the window length below 30 s, they disappear, which indicates that these spectral lines are not a tremor signal, as tremor would be visible regardless of the window length. This analysis suggests the existence of a repetitive source acting every ∼30 s. The distance between spectral lines is ∼0.027 Hz at MNAI and ∼0.02 Hz at BLSI. Following the relation in Powell and Neuberg (2003) or Hotovec et al. (2013) at Soufrière Hills and Redoubt volcanoes respectively, the spacing between the spectral lines suggests regular excitation every 30–50 s. Audible explosions, every ∼30 s, were recorded previously at Anak Krakatau from Rakata Island (Fig. 1), ∼4 km away, which suggests that a repeated explosive source on the order of 30–50 s is plausible for Anak Krakatau. The infrasound network MARP, during favorable conditions, continued to record activity from Anak Krakatau after the collapse, and recorded a repetitive signal consistent with a Surtseyan explosion, with an occurrence on the order of 1 min, consistent with the expected temporal spacing expected based on the spectral distance.

5.4. Conceptual model of timeline

By combining the official reported activity with remote geophysical observations and eyewitness accounts, a more detailed picture of the eruption chronology can be compiled (Fig. 5). Reported time for seismic and infrasound are back-propagated to the vent using 1 km/s nominal seismic velocity and the calculated 0.2902 km/s infrasound celerity. The initial phase of the eruption, Phase 0, began June 2018 and ended December 22. Phase 1 began on December 22 and continued until December 30. It was characterized by a dramatic change in both eruptive style and edifice morphology.

Phase 1A began on December 22 circa 05:30 (Infra1), and was characterized by sustained eruptive activity consisting of intense Strombolian lava fountaining and ash rich plumes (Official reports and Photo1). For the majority of this Phase (lasting until the collapse at 13:55) the view of the Anak Krakatau from satellite was obscured by meteorological clouds (Himawari-8 and Photo1), with sustained infrasound continuing throughout. Around 10:30, a lava flow began near the summit, likely due to the tephra accumulation from lava fountaining, and by ∼11:00 there is a clear interaction of this lava with the sea on the South flank (Photo3). Around 12:50 there were two seismic signals (Seis1a and Seis1b) consistent with possible small scale slides, however, as they are only recorded on the closest station with no direct visual observations, they cannot be confirmed. There is a vague plume reported at 13:10 by the Darwin VAAC. The infrasound signals suggest activity continued without much change until ∼13:30 (Infra2) when a gap in remote infrasound detection coincides with the reported lack of audible activity (eyewitness), which likely indicates a pause or change in activity at the surface. After the gap the infrasound detection resumed at a similar level as before. The infrasound within this phase, while strong, is similar to infrasound recorded during a similar episode of heightened activity in early October 2018 which also included lava flows reaching the sea (Fig. A.14).

Phase 1B, the collapse, occurred ∼13:55. The largest signals in both seismic and infrasound records are associated to the collapse and main mass loss event (Seis3, and Infra3) which was also recorded as a M5.1 from the GEOFON automatic detection system. The infrasound signal was recorded as multiple arrivals at the station I06AU (Infra 3, Infra3a, and Infra3b). Seismic signal Seis2 is likely due to the initial pulse of this collapse, indicating a more complex geometry than proposed by Grilli et al. (2019), and beginning before the commonly cited 13:55 time associated with the large signal Seis3. However, as with the earlier signals Seis1a and Seis1b, due to this signal only being recorded on the closest station, it cannot be confirmed this flank collapse is what generated the tsunami. This dramatic change in morphology can be seen in the Sential-1A (Sat7) and ALOS-2 overflights, as well as the commercial overflight on December 23. This changed the dynamic from intense Strombolian activity to sustained Surtseyan as seawater infiltrated the vent (Williams et al., 2019), and continued with a sustained but pulsing plume until December 28 (Infra4, Seis6).

Phase 1C began directly after the collapse and included the three initial large eruptive pulses: one directly after the collapse at 13:55, lasting ∼1 h (Sat3), a second at 15:25, lasting ∼20 min (Sat4), and a third at 15:55, lasting ∼50 min (Sat5). These three pulses are reported by the fishermen, and the relative timing observed in satellite is consistent with their account. These intense eruptions and the following sustained activity are likely due to the unroofing and depressurization of the magma storage region, and the introduction of sea water to the active vent area. This follows the model proposed for cycles of failures and more intense eruptions by Hunt et al. (2018) based on island and terrestrial examples.

After these distinct pulses, the eruption entered Phase 1D at 16:55 (Sat6), characterized by a sustained plume with fluctuations in intensity and detectable SO_2 (Sat8). This activity produced a plume that consistently rose 16 km above sea level for the entire 7 days of Phase 1D (Darwin VAAC reports and satellite post processing). The frequency of the pulses was derived from the distance between the seismic spectral lines, which resulted in an explosion every ∼50 s, with intermittent larger events (Seis6). Signals recorded at MARP after the collapse are consistent with a repetitive Surtseyan explosion source as seen at Bogoslof (Lyons et al., 2019).

The sustained plume ceased at approximately 05:05 (Sat9), December 28, and Phase 1E beginning at this time is characterized by a ramping down of the geophysical observations. The seismic signal ceases, and the number of infrasound detections decreases significantly, SO_2 is no longer observed by the 05:20 scan on the 28th, thus bringing an end to Phase 1 of this eruption by December 30th. Within this proposed model, this would signify stabilization, and return to pre-collapse conditions for the magma storage region.

This unique combination of datasets allowed us to build a detailed chronology, and while it is in broad agreement with other studies, there are some key differences. We identified three main, distinct plumes before a transition to a continuous eruptive plume. Most studies did not explicitly address the number of plumes (Walter et al., 2019; Williams et al., 2019; Prata et al., 2020; Gouhier and Paris, 2019) or cited only two (Ye et al., 2020). Our study indicates that there was one failure and not multiple failures like proposed by Williams et al. (2019), and no evidence for a "trigger" (earthquake or explosion) prior to the collapse as proposed by Walter et al. (2019). This seismo-acoustic signal of a well constrained event can aid in development of automated detection systems for volcanic flank collapse and other tsuanmigenic landslides (Nuugaatsiaq, Greenland Butler, 2019).

6. Conclusions

Volcano related tsunamis are a major global hazard, albeit with very limited number of direct observations (Watt et al., 2019; Paris et al., 2014; Grilli et al., 2019). In this case, although the local monitoring system was destroyed, remote geophysical and satellite data, together with eye-witnesses accounts, allowed us to reconstruct the sequence of events on December 22, 2018. This detailed

reconstruction suggests that remote seismo-acoustic observations can provide critical information on hazardous events that would otherwise be difficult to obtain, which emphasizes the importance of complementing local networks with regional geophysical and remote sensing. This detailed sequence, leading to tsunamigenic flank collapse, is rarely observed and provides data that could be used to understand how, or if, it could have been identified in real-time. Such observations are crucial to enhanced monitoring for similar fast growing, steep volcanoes around the world, and to help mitigate their hazards.

Disclaimer

The views expressed in this study are those of the authors and do not necessarily reflect those of the Preparatory Commission for the CTBTO.

Declaration of competing interest

The authors declare that they have no known competing financial interests or personal relationships that could have appeared to influence the work reported in this paper.

Acknowledgements

The authors would like to acknowledge the assistance of the following individuals and organizations. We would like to thank Andrew Prata and Pete Webley for assistance in procurement and interpretation of Himawari-8 data, and JMA for access to the Himawari-8 data, as well as BMKG for providing seismic data for this project. We would also like to thank Christina Widiwijayanti for translation assistance for the fisherman's accounts. We would also like to thank Pavel Adamek for editorial assistance, especially with the eyewitness reports section. We would also like to thank Rebecca Williams and three anonymous reviewers for their comments which substantially improved the manuscript. Waveform data are available through IRIS, Data Services (NSF Cooperative Support Agreement EAR-1851048), the vDEC platform of the International Data Center, and BMKG upon request. Satellite imagery is available through the agencies responsible. The authors would also like to offer their deepest condolences to all those impacted by this eruption and tsunami. This work comprises Earth Observatory of Singapore contribution No. 250. This research is partly supported by the National Research Foundation Singapore and the Singapore Ministry of Education under the Research Centres of Excellence initiative.

Appendix. Supplementary material

Supplementary material related to this article can be found online at https://doi.org/10.1016/j.epsl.2020.116268.

References

Albersheim, S., Guffanti, M., 2009. The United States national volcanic ash operations plan for aviation. Nat. Hazards 51 (2), 275–285. https://doi.org/10.1007/s11069-008-9247-1.

Allstadt, K., 2013. Extracting source characteristics and dynamics of the August 2010 Mount Meager landslide from broadband seismograms. J. Geophys. Res., Earth Surf. 118 (3), 1472–1490.

Allstadt, K.E., Matoza, R.S., Lockhart, A.B., Moran, S.C., Caplan-Auerbach, J., Haney, M.M., Thelen, W.A., Malone, S.D., 2018. Seismic and acoustic signatures of surficial mass movements at volcanoes. J. Volcanol. Geotherm. Res. 364, 76–106. https://doi.org/10.1016/j.jvolgeores.2018.09.007.

ALOS-2 Project, 2018. JAXA/EORC ALOS PALSAR ALOS-2. http://www.eorc.jaxa.jp/ALOS/en/top/about_top.htm.

AP Archive, 2018. Indonesia volcano (CR): aerial video of Indonesia volcano eruption. Retrieved from http://www.aparchive.com/metadata/youtube/377ebcaaaf1d2d0ceef1a9afe7dc74bd.

Babu, A., Kumar, S., 2019. InSAR coherence and backscatter images based analysis for the Anak Krakatau volcano eruption. Proceedings 2. https://doi.org/10.3390/IECG2019-06216.

Bachelet, V., Mangeney, A., De Rosny, J., Toussaint, R., Farin, M., 2018. Elastic wave generated by granular impact on rough and erodible surfaces. J. Appl. Phys. 123 (4), 044901.

Bessho, K., Date, K., Hayashi, M., Ikeda, A., Imai, T., Inoue, H., Kumagai, Y., Miyakawa, T., Murata, H., Ohno, T., Okuyama, A., Oyama, R., Sasaki, Y., Shimazu, Y., Shimoji, K., Sumida, Y., Suzuki, M., Taniguchi, H., Tsuchiyama, H., Uesawa, D., Yokota, H., Yoshida, R., 2016. An introduction to Himawari-8/9 – Japan's new-generation geostationary meteorological satellites. J. Meteorol. Soc. Jpn. 94 (2), 151–183. https://doi.org/10.2151/jmsj.2016-009.

BMKG Data Centre, 2015. BMKG Indonesian seismic network. http://inatews.bmkg.go.id/new/query_gmpqc.php.

Butler, R., 2019. Seismic precursors to a 2017 Nuugaatsiaq, Greenland, earthquake–landslide–tsunami event. Nat. Hazards 96, 961–973. https://doi.org/10.1007/s11069-019-03582-8.

Cansi, Y., 1995. An automatic seismic event processing for detection and location: the P.M.C.C. method. Geophys. Res. Lett. 22, 1021–1024. https://doi.org/10.1029/95GL00468.

Ceranna, L., Le Pichon, A., Green, D.N., Mialle, P., 2009. The Buncefield explosion: a benchmark for infrasound analysis across Central Europe. Geophys. J. Int. 177 (2), 491–508. https://doi.org/10.1111/j.1365-246X.2008.03998.x.

Christie, D.R., Campus, P., 2010. The IMS infrasound network: design and establishment of infrasound stations. In: Le Pichon, A., Blanc, E., Hauchecorne, A. (Eds.), Infrasound Monitoring for Atmospheric Studies. Springer, New-York, pp. 3–27.

Coombs, M.L., Wech, A.G., Haney, M.M., Lyons, J.J., Schneider, D.J., Schwaiger, H.F., Wallace, K.L., Fee, D., Freymueller, J.T., Schaefer, J.R., Tepp, G., 2018. Short-term forecasting and detection of explosions during the 2016-2017 eruption of Bogoslof volcano, Alaska. Front. Earth Sci. https://doi.org/10.3389/feart.2018.00122.

Copernicus Sentinel Data, 2018. https://sentinels.copernicus.eu/documents/247904/690755/Sentinel_Data_Legal_Notice.

Darwin Volcanic Ash Advisory Center (VAAC), 2018. Bureau of meteorology. Alert archive available at ftp://ftp.bom.gov.au/anon/gen/vaac/.

Dziak, R.P., Park, M., Matsumoto, H., Byun, S.K., 2005. Hydroacoustic records and a numerical model of the source mechanism from the first historical eruption of Anatahan volcano, Mariana Islands. J. Volcanol. Geotherm. Res. 146 (1–3), 86–101. https://doi.org/10.1016/j.jvolgeores.2004.12.009.

Ekström, G., Stark, C.P., 2013. Simple scaling of catastrophic landslide dynamics. Science 339 (6126), 1416–1419.

ESDM, 2018a. Pers Rilis Aktivitas Gunungapi Anak Krakatau, Rabu 3 Oktober 2018. Retrieved Aug. 13, 2019, from http://www.vsi.esdm.go.id/index.php/gunungapi/aktivitas-gunungapi/2445-pers-rilis-aktivitas-gunungapi-anak-krakatau-rabu-3-oktober-2018.

ESDM, 2018b. Tanggapan Kejadian Tsunami Di Selat Sunda, Tanggal 22 Desember 2018. Retrieved Feb. 18, 2019, from https://www.esdm.go.id/id/media-center/arsip-berita/tanggapan-kejadian-tsunami-di-selat-sunda-tanggal-22-desember-2018.

Evers, L.G., Haak, H.W., 2010. The characteristics of infrasound, its propagation and some early history. In: Le Pichon, A., Blanc, E., Hauchecorne, A. (Eds.), Infrasound Monitoring for Atmospheric Studies. Springer, New-York, pp. 3–27.

Farin, M., Mangeney, A., Toussaint, R., de Rosny, J., Shapiro, N., Dewez, T., Hibert, C., Mathon, C., Sedan, O., Berger, F., 2015. Characterization of rockfalls from seismic signal: insights from laboratory experiments. J. Geophys. Res., Solid Earth 120 (10), 7102–7137. https://doi.org/10.1002/2015JB012331.

Farin, M., Mangeney, A., de Rosny, J., Toussaint, R., Trinh, P.T., 2019. Relations between the characteristics of granular column collapses and resultant high-frequency seismic signals. J. Geophys. Res., Earth Surf.

Fee, D., Lyons, J., Haney, M., Wech, A., Waythomas, C., Diefenbach, A.K., Lopez, T., Van Eaton, A., Schneider, D., 2020. Seismo-acoustic evidence for vent drying during shallow submarine eruptions at Bogoslof volcano, Alaska. Bull. Volcanol. 82 (2). https://doi.org/10.1007/s00445-019-1326-5.

Garces, M., 2013. On infrasound standards, part 1: time, frequency, and energy scaling. InfraMatics 2 (2), 13–35.

GEOFON Data Centre, 1993. The GEOFON seismic network. Deutsches GeoForschungsZentrum GFZ. Other/Seismic Network. https://doi.org/10.14470/TR560404.

GEOFON Data, 2018. Moment tensor solutions in the Sunda Strait, Indonesia, on December 22, 2018. Deutsches GeoForschungsZentrum GFZ. Other/Seismic Network. http://geofon.gfz-potsdam.de/eqinfo/event.php?id=gfz2018yzre.

Giachetti, T., Paris, R., Kelfoun, K., Ontowirjo, B., 2012. Tsunami hazard related to a flank collapse of Anak Krakatau Volcano, Sunda Strait, Indonesia. J. Geol. Soc. Lond. 361 (Special Publications), 79–90. https://doi.org/10.1144/SP361.7.

Global Volcanism Program, 2013. Krakatau (262000) in Volcanoes of the World (VOTW) database information. In: Venzke, E. (Ed.), Smithsonian Institution. https://doi.org/10.5479/si.GVP.VOTW4-2013, Version 4.7.7. https://volcano.si.edu/volcano.cfm?vn=262000. (Accessed 16 April 2019).

Global Volcanism Program, 2018. Report on Krakatau (Indonesia). In: Sennert, S.K. (Ed.), Weekly Volcanic Activity Report. 20 June-26 June 2018. Smithsonian Institution and US Geological Survey. https://volcano.si.edu/showreport.cfm?doi=GVP.WVAR20180620-262000.

Gouhier, M., Paris, R., 2019. SO2 and tephra emissions during the December 22, 2018 Anak Krakatau eruption. Volcanica 2 (2), 91–103. https://doi.org/10.30909/vol.02.02.91103.

Grilli, S.T., Tappin, D.R., Carey, S., Watt, S.F.L., Ward, S.N., Grilli, A.R., Engwell, S.L., Zhang, C., Kirby, J.T., Schambach, L., Muin, M., 2019. Modelling of the tsunami from the December 22, 2018 lateral collapse of Anak Krakatau volcano in the Sunda Straits, Indonesia. Sci. Rep. 9, 11946. https://doi.org/10.1038/s41598-019-48327-6.

Hibert, C., Ekström, G., Stark, C.P., 2014. Dynamics of the Bingham Canyon Mine landslides from seismic signal analysis. Geophys. Res. Lett. 41 (13), 4535–4541. https://doi.org/10.1002/2014GL060592.

Hibert, C., Stark, C.P., Ekström, G., 2015. Dynamics of the Oso-Steelhead landslide from broadband seismic analysis. Nat. Hazards Earth Syst. Sci. 15 (6), 1265–1273. https://doi.org/10.5194/nhess-15-1265-2015.

Hibert, C., Ekström, G., Stark, C.P., 2017. The relationship between bulk-mass momentum and short-period seismic radiation in catastrophic landslides. J. Geophys. Res., Earth Surf. 122 (5), 1201–1215. https://doi.org/10.1002/2016JF004027.

Himawari Cloud Dataset, 2015. Full-disk Himawari standard data and HRIT data. MSC of JMA. http://www.data.jma.go.jp/mscweb/en/himawari89/cloud_service/cloud_service.html. Data available from 2015.

Hotovec, A.J., Prejean, S.G., Vidale, J.E., Gomberg, J.S., 2013. Strongly gliding harmonic tremor during the 2009 eruption of Redoubt volcano. J. Volcanol. Geotherm. Res. 259 (Redoubt Special Issue), 89–99. https://doi.org/10.1016/j.jvolgeores.2012.01.001.

Hunt, J.E., Cassidy, M., Talling, P.J., 2018. Multi-stage volcanic island flank collapses with coeval explosive caldera-forming eruptions. Sci. Rep. 8 (1), 1146. https://doi.org/10.1038/s41598-018-19285-2.

Kanamori, H., Given, J.W., 1982. Analysis of long-period seismic waves excited by the May 18, 1980, eruption of Mount St. Helens – a terrestrial monopole? J. Geophys. Res., Solid Earth 87 (B7), 5422–5432. https://doi.org/10.1029/JB087iB07p05422.

Kristianto, 1999. New Monitoring Technique for Active Volcanoes: Part 1. Infrasonic Monitoring of Strombolian Activity at Krakatau Volcano. Japan International Cooperation Agency Report.

Kristianto, Triastuty, H., Mulyana, I., Rosadi, U., Basuki, A., 2019. Revitalization of early warning systems of the Anak Krakatau volcano eruption post-eruption 2018. In: The 6th Annual Scientific Meeting on Disaster Research 2019 International Conference on Disaster Management. In: Proceeding Book, vol. 4, p. 150.

Lampung TV, 2018. 16 Jam di Pusaran Letusan Krakatau dan Tsunami Lampung. Retrieved Dec. 27, 2018, from https://youtu.be/Ampw9lUBOCY.

Lampung TV, T.V., 2019. Saksikan Air Laut Kering Disedot Krakatau saat Tsunami. Retrieved Jan. 4, 2019, from https://www.youtube.com/watch?v=KtR0x_FfJfE.

Lyons, J.J., Haney, M.M., Fee, D., Wech, A.G., Waythomas, C.F., 2019. Infrasound from giant bubbles during explosive submarine eruptions. Nat. Geosci. 12 (11), 952–958. https://doi.org/10.1038/s41561-019-0461-0.

Lyons, J., Iezzi, A.M., Fee, D., Schwaiger, H.F., Wech, A.G., Haney, M.M., 2020. Infrasound generated by the 2016–2017 shallow submarine eruption of Bogoslof volcano, Alaska. Bull. Volcanol. 82 (2), 19.

Matoza, R.S., Fee, D., Neilsen, T.B., Gee, K.L., Ogden, D.E., 2013. Aeroacoustics of volcanic jets: acoustic power estimation and jet velocity dependence. J. Geophys. Res., Solid Earth 118 (2), 6269–6284. https://doi.org/10.1002/2013JB010303.

Metz, D., Grevemeyer, I., 2018. Hydroacoustic measurements of the 2014 eruption at Ahyi volcano, 20.4°N, Mariana. Arc. Geophys. Res. Lett. 45 (20), 050. https://doi.org/10.1029/2018GL079983.

Mutaqin, B.W., Lavigne, F., Hadmoko, D.S., Ngalawani, M.N., 2019. Volcanic eruption-induced tsunami in Indonesia: a review. In: IOP Conference Series. Environ. Earth Sci. 256, 012023. https://doi.org/10.1088/1755-1315/256/1/012023.

Newhall, C.G., Endo, E.T., 1987. Sudden seismic calm before eruptions: illusory or real? In: Abstract Volume, Hawaii Symposium on How Volcanoes Work. Hilo, Hawaii. 190 pp.

Nugroho, S.P., 2018a. Volume Tubuh Gunung Anak Krakatau Berkurang, Jumlah Korban Tsunami Bertambah. Retrieved May 6, 2019, from https://bnpb.go.id/volume-tubuh-gunung-anak-krakatau-berkurang-jumlah-korban-tsunami-bertambah.

Nugroho, S.P., 2018b. 6) Jaringan buoy tsunami di perairan Indonesia sudah tidak beroperasi sejak 2012. Retrieved Dec. 23, 2018, from https://twitter.com/Sutopo_PN/status/1077003132545118208.

Nugroho, S.P., 2018c. Erupsi Gunung Anak Krakatau yang terpantau dari pesawat Grand Caravan Susi Air pada 23/12/2018. Retrieved Dec. 23, 2019, from https://twitter.com/Sutopo_PN/status/1077005337780080642.

Nugroho, S.P., 2018d. Erupsi Gunung Anak Krakatau yang terpantau dari pesawat Grand Caravan Susi Air pada 23/12/2018. Retrieved Dec. 23, 2019, from https://twitter.com/Sutopo_PN/status/1077045675290812416.

Paris, R., Switzer, A.D., Belousova, M., Belousov, A., Ontowirjo, B., Whelley, P.L., Ulvrova, M., 2014. Volcanic tsunami: a review of source mechanisms, past events and hazards in Southeast Asia (Indonesia, Philippines, Papua New Guinea). Nat. Hazards 70 (1), 447–470. https://doi.org/10.1007/s11069-013-0822-8.

Powell, T.W., Neuberg, J.W., 2003. Time dependent features in tremor spectra. J. Volcanol. Geotherm. Res. 128 (1–3), 177–185. https://doi.org/10.1016/S0377-0273(03)00253-1.

Prata, A.T., Folch, A., Prata, A.J., Biondi, R., Brenot, H., Cimarelli, C., Corradini, S., Lapierre, J., Costa, A., 2020. Anak Krakatau Triggers volcanic freezer in the upper troposphere. Sci. Rep. 10 (1), 3584. https://doi.org/10.1038/s41598-020-60465-w.

Roman, D.C., Rodgers, M., Geirsson, H., LaFemina, P.C., Tenorio, V., 2016. Assessing the likelihood and magnitude of volcanic explosions based on seismic quiescence. Earth Planet. Sci. Lett. 450, 20–28. https://doi.org/10.1016/j.epsl.2016.06.020.

Simkin, T., Fiske, R.S., 1983. Krakatau, 1883: The Volcanic Eruption and Its Effects. Smithsonian Institution Press, Washington D.C. ISBN 0874748410. 464 pp. (Second printing 1984).

Smart, E., Flinn, E.A., 1971. Fast frequency-wavenumber analysis and Fisher signal detection in real-time infrasonic array data processing. Geophys. J. Int. 26 (1–4), 279–284. https://doi.org/10.1111/j.1365-246X.1971.tb03401.x.

Strachey, R., 1888. On the air waves and sounds caused by the eruption of Krakatoa in August, 1883. In: Symons, G.J. (Ed.), The Eruption of Krakatoa and Subsequent Phenomena, Report of the Krakatoa Committee of the Royal Society. Trubner and Co., London, pp. 57–88.

Syamsidik, Benazir, Luthfi, M., Suppasri, A., Comfort, L.K., 2020. The 22 December 2018 mount Anak Krakatau volcanogenic tsunami on Sunda Strait coasts, Indonesia: tsunami and damage characteristics. Nat. Hazards Earth Syst. Sci. https://doi.org/10.5194/nhess-2019-252.

TvOneNews, 2018. Terdampar 7 Hari di Pulau Terpencil, Seorang Nelayan Berhasil Selamat Terdampar 7 Hari di Pulau Terpencil, Seorang Nelayan Berhasil Selamat Dari Tsunami Selat Sunda. Retrieved Dec. 31, 2018, from https://www.youtube.com/watch?v=yQMajvJh59g.

Verbeek, R.D.M., 1884. The Krakatau eruption 1. Nature 30, 10–15. https://doi.org/10.1038/030010a0.

Walter, T.R., Haghshenas Haghighi, M., Schneider, F.M., Coppola, D., Motagh, M., Saul, J., Babeyko, A., Dahm, T., Troll, V.R., Tilmann, F., Heimann, S., Valade, S., Triyono, R., Khomarudin, R., Kartadinata, N., Laiolo, M., Massimetti, F., Gaebler, P., 2019. Complex hazard cascade culminating in the Anak Krakatau sector collapse. Nat. Commun. 10 (1), 4339. https://doi.org/10.1038/s41467-019-12284-5.

Watt, S.F.L., Karstens, J., Micallef, A., Berndt, C., Urlaub, M., Ray, M., Desai, A., Sammartini, M., Klaucke, I., Böttner, C., Day, S., Downes, H., Kühn, M., Elger, J., 2019. From catastrophic collapse to multi-phase deposition: flow transformation, seafloor interaction and triggered eruption following a volcanic-island landslide. Earth Planet. Sci. Lett. 517 (July), 135–147. https://doi.org/10.1016/j.epsl.2019.04.024.

Waxler, R., Assink, J., Hetzer, C., Velea, D., 2017. NCPAprop – a software package for infrasound propagation modeling. J. Acoust. Soc. Am. 141 (5), 3627. https://doi.org/10.1121/1.4987797.

Waxler, R., Assink, J., 2019. Propagation modeling through realistic atmosphere and benchmarking. In: Le Pichon, A., Blanc, E., Hauchecorne, A. (Eds.), Infrasound Monitoring for Atmospheric Studies. Springer, New-York, pp. 509–549.

Williams, R., Rowley, P., Garthwaite, M.C., 2019. Reconstructing the Anak Krakatau flank collapse that caused the December 2018 Indonesian tsunami. Geology. https://doi.org/10.1130/G46517.1.

Ye, L., Kanamori, H., Rivera, L., Lay, T., Zhou, Y., Sianipar, D., Satake, K., 2020. The 22 December 2018 tsunami from flank collapse of Anak Krakatau volcano during eruption. Sci. Adv. 6 (3). https://doi.org/10.1126/sciadv.aaz1377.

Yokoo, A., Iguchi, M., Tameguri, T., Yamamoto, K., 2013. Processes prior to outbursts of vulcanian eruption at Showa crater of Sakurajima volcano. Bull. Volcanol. Soc. Jpn. 58, 163–181.